Fuel 137 (2014) 11–20

Contents lists available at ScienceDirect

Fuel

journal homepage: www.elsevier.com/locate/fuel

Combustion analysis of an equimolar mixture of methane and syngas in a surface-stabilized combustion burner for household appliances

Carlos E. Arrieta *, Andrés A. Amell

Science and Technology of Gases and Rational Use of Energy Group, Faculty of Engineering, University of Antioquia UdeA, Calle 70 No. 52-21, Medellín, Colombia

HIGHLIGHTS

- Combustion of methane–syngas were studied in a ceramic surface-stabilized combustion burner.
- The present study evaluates a high hydrogen content syngas.
- The overall flame structure was visualized with OH chemiluminescence.
- Radiation efficiencies were obtained from a radiometer measurements methodology.
- This type of burner exhibits a great potential for interchangeable use of gas fuels.

ARTICLE INFO

Article history:
Received 28 April 2014
Received in revised form 24 July 2014
Accepted 24 July 2014
Available online 5 August 2014

Keywords:
Surface-stabilized combustion
Methane
Syngas
High hydrogen content syngas
Household appliances

ABSTRACT

The primary objective of this work is to study the combustion of an equimolar mixture of methane and syngas (CH_4–*SG*) in a ceramic surface-stabilized combustion burner. We examine the effects of the fuel composition, the air-to-fuel ratio and the thermal input on the flame stability, the radiation efficiency and the pollutant emissions (CO and NOx). In this study, we evaluate a syngas with a high hydrogen content that is similar to those obtained by coal gasification (50–60% H_2) using Sasol/Lurgi gasification technology and biomass gasification, for example. To determine the effect of the air-to-fuel ratio (λ), the burner performance is analyzed at $\lambda = 1.4$ and $\lambda = 1.1$. Some studies have reported optimal operating conditions for $\lambda = 1.4$, whereas for hydrocarbons, the proximity to stoichiometric conditions at the $\lambda = 1.1$ air-to-fuel ratio produces the highest possible laminar burning velocity and flame temperature. The thermal inputs evaluated in this study correspond to three values (1.0, 1.8, and 2.5 kW) found in household appliances and for cooking appliances in particular. The results for this experimental burner design indicate that the macroscopic flame shape for an equimolar CH_4–*SG* mixture is approximately the same as that for CH_4. Moreover, the pollutant concentrations in the flue gas are generally below 85 ppm for CO and 15 ppm for NOx. However, the thermal input and the air-to-fuel ratio significantly affect the flame structure, the radiation efficiency and the pollutant emissions.

© 2014 Elsevier Ltd. All rights reserved.

1. Introduction

Recent reports have shown that industrial level combustion processes in which the energy sources are generally solid, liquid and gaseous non-renewable fuels have become cleaner and more efficient through the use of new technologies such as heat recovery and flameless combustion [1].

Natural gas (*NG*), which consists primarily of CH_4, is commonly used in household appliances such as heating and cooking units. *NG* is considered to be a clean fuel compared to other fossil fuels. However, *NG* produces CO_2, CO and NOx. CO_2 emissions are inherent to the combustion of fossil fuels and can only be reduced by improving the efficiency of the equipment. CO is associated with incomplete combustion; thus, increasing efficiency levels may decrease CO values to near zero. NOx emission is inherent to combustion with air and requires high temperatures in the reaction zone [2,3].

In Colombia, *NG* consumption by the residential sector has grown at a rapid pace in recent years. Recent reports have shown that in 2012, 460,918 new households were integrated into the domiciliary *NG* distribution network (which was double the expected number of households) for a total of 960,000 new households in the last two years. This growth is expected to increase *NG* consumption further [4]. Considering the current conditions for the

* Corresponding author.
E-mail addresses: carlosarrieta@udea.edu.co, carlos.e.arrieta@gmail.com (C.E. Arrieta), anamell@udea.edu.co (A.A. Amell).

http://dx.doi.org/10.1016/j.fuel.2014.07.079
0016-2361/© 2014 Elsevier Ltd. All rights reserved.

Nomenclature

SG	synthesis gas or syngas
CH_4–*SG*	equimolar mixture of methane and syngas
λ	air-to-fuel ratio
V_U	unburnt gas velocity (cm/s)
S_L	adiabatic laminar burning velocity (cm/s)
Po	thermal input (kW)
LHV	lower heating value (kW h/m^3_{st}), where st denotes standard
$V_{a,sto}$	volumetric air requirement for stoichiometric combustion (m^3_{air}/m^3_{fuel})
Wo	Wobbe index based on high heating value (kW h/m^3_{st})
Tad	adiabatic flame temperature (K)
ϕ	porosity
A_{sup}	surface area of burner (m^2)
p	thickness of porous media (mm)
CO_{2max}	maximum CO_2 fraction at stoichiometric conditions
$(CO/CO_2)_{sample}$	ratio of CO to CO_2, as measured in the analyzer
n_R	radiation efficiency
Po_{rad}	radiant power output (kW)
$\dot{V}_{air}$	air flow rate (slpm)
ε	emissivity of the burner surface
σ	Stefan–Boltzmann constant, $\sigma = 5.6704 \times 10^{-8} W/m^2K^4$
T_{sup}	temperature at the surface of the burner (K)

exploration and exploitation of *NG* resources, supply forecasts estimate that Colombian fuel reserves will be exhausted in the next 18 years [5].

Consequently, previous research has focused on increasing process efficiencies and developing alternative fuels, which is of great interest to countries and regions with reserves of other alternative energy sources. *Synthetic gas* (syngas, *SG*) obtained from the gasification of coal and biomass is considered to be one of the most promising alternative fuels in developed and developing countries [6–8]. Syngas is expected to play an important role in diversifying the energy supply in Colombia, which has the highest carbon reserves in Latin America and considerable availability of organic waste and biomass for gasification in rural areas [9]. However, depending on the type of reactor and the gasifying agent, syngas generally has lower heating values between 1.0 and ~2.6 kW h/m^3 and Wobbe index values between 1.5 and ~4 kW h/m^3, which are very low compared to the values for pure CH_4 (9.425 kW h/m^3 and 14.09 kW h/m^3, respectively). Thus, there is a strong global effort to burn mixtures of conventional fuels and syngas, which also provides alternatives to increase the use of available fuels [10].

Systems that include preheating of the reactant mixture have been shown to increase the stability range and facilitate effective combustion in these fuel mixtures [11,12]. One way of designing a burner with internal heat recirculation is to stabilize a premixed flame on the surface of porous inert media [13,14]. The energy released by the reaction is transferred to the porous surface, which in turn emits the energy to its surroundings (such as in radiant burners) and conducts the energy upstream to preheat the reactants in the preheat zone. Since the 1990s, many studies have shown the benefits of using this technique in combustion processes with high thermal powers [13,15–17]. Recent studies have demonstrated that these benefits (high thermal efficiencies, low pollutant emissions and fuel interchangeability) can also be obtained at low thermal powers [13,18,19]. Yu et al. [20] studied the behavior of a 5.8-kW surface-stabilized combustion burner in a water heater fueled with *NG*. The burner surface consisted of a perforated steel plate (AISI 304) with a porosity of 83%. Low pollutant emissions and high efficiencies (~79.7%) were achieved by operating the burner at an air-to-fuel ratio slightly higher than 1.3. Recently, the same authors [21] evaluated a similar device but varied the material of the burner surface using perforated steel (31% porosity) and ceramic aluminum oxide plates (49.5% porosity). Using a ceramic surface increased the thermal efficiency to nearly 85% but did not significantly change the emissions levels. Keramiotis et al. [22] also obtained low pollutant emissions levels using an alumina ceramic burner fueled with *NG* and *LPG*. The authors evaluated the CO and NOx emissions for two thermal power levels (4 kW and 8 kW) and three air-to-fuel ratios (1.2, 1.4 and 1.6). In all of the cases considered, the emissions were considerably reduced for air-to-fuel ratios greater than 1.2, which is in agreement with a previous study by Yu et al. [20,21]. Both fuels yielded CO and NOx concentrations of 10 ppm and 5 ppm, respectively. The ceramic burners also improved the flame stability by allowing interchangeability between natural gas and LPG. Wu et al. [23] studied the performance of a metal surface-stabilized combustion burner in a cooking appliance and found that the thermal efficiency was higher than that of a conventional Bunsen burner. However, the thermal efficiency was lower than those reported for ceramic burners.

The primary objective of this study is to compare the combustion of CH_4 with an equimolar mixture of CH_4 and *SG* in a ceramic surface-stabilized combustion burner. We examine the effect of the fuel composition, the air-to-fuel ratio and the thermal power input on the flame stability and pollutant emissions. We evaluate a high hydrogen *SG* similar to those obtained from coal gasification by Sasol/Lurgi gasification [24] and biomass gasification [25]. To determine the effect of the air-to-fuel ratio (λ), the burner performance is analyzed at $\lambda = 1.4$ and $\lambda = 1.1$. Some studies have reported optimal operating conditions for air-to-fuel ratios values near 1.4 [20], whereas $\lambda = 1.1$ offers the advantage of being near the stoichiometric conditions at which hydrocarbons have the highest possible S_L and *Tad*.

2. Experimental methodology

2.1. Operation modes of a surface-stabilized combustion burner

The operation of a surface-stabilized combustion burner can be characterized using the ratio of the laminar burning velocity of the fuel to the unburned gas velocity. When V_U is lower than S_L, the flame propagates upstream until the flame reaches the burner surface. The flame is then cooled by the burner, which reduces S_L until it equals V_U. Finally, a flat flame stabilizes close to or even partly within the burner, as shown in Fig. 1a. The flame temperature is reduced, which significantly decreases the production of thermal NOx. The energy emitted by the flame heats the porous media, which radiate the energy to the surroundings and preheats the unburned gas. A second operation mode is identified when V_U increases to values near S_L. Bouma [26] showed that two-fold flame behavior occurs under this condition. There are regions where V_U exceeds S_L. In these regions, a Bunsen-type flame occurs, and the distance between the flame and the burner surface increases. Consequently, the burner surface temperature decreases. At other positions, the flame stabilizes close to the burner and heats the surface, as shown in Fig. 1b. Under this operation condition (i.e., $\sim V_U/S_L > 1$), the flame temperature is expected to increase, changing the NOx emissions from those produced in the former

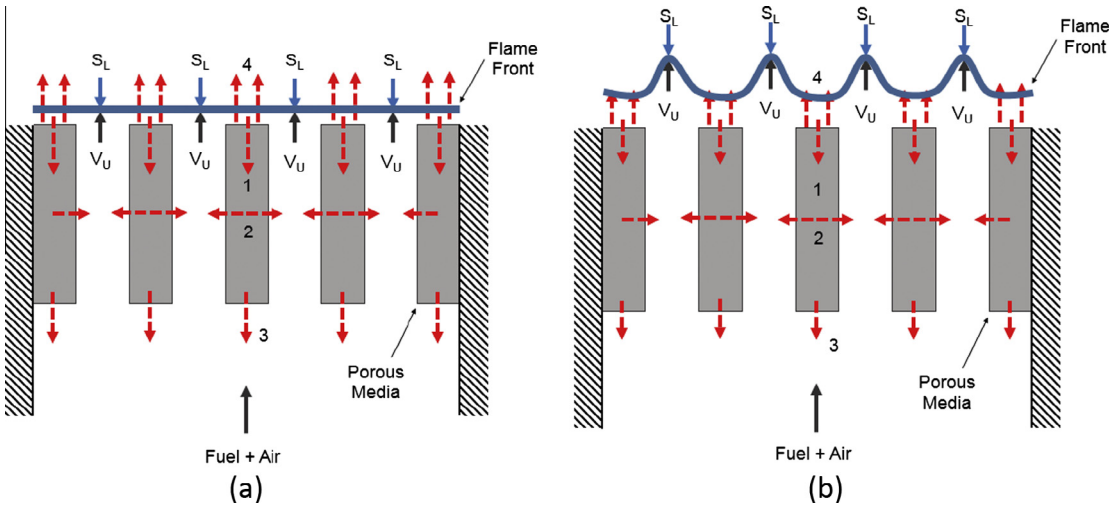

Fig. 1. A representation of the operation mode of a surface-stabilized combustion burner. (a) V_U lower than S_L; (b) S_L lower than V_U. 1 – heat loss from the flame to the burner. 2 and 3 – heat transfer from the burner to the unburned gas. 4 – heat transfer from the burner surface to the surroundings.

operation mode (i.e., $\sim V_U/S_L < 1$). When V_U is much higher than S_L, the flame blows out.

V_U is determined using the following relationship between V_U, Po, LHV, λ and $V_{a,sto}$.

$$V_U = 0.028 \frac{Po}{\phi A_{sup} LHV} [1 + \lambda V_{a,sto}] \quad (1)$$

Eq. (1) shows that a change in the fuel composition affects V_U via the fuel energy content and the air quantity requirements. Therefore, these two variables are expected to have strong effects on the burner operation when CH_4–SG is used. These two variables should also affect S_L and Tad.

2.2. Experimental configuration

Fig. 2 is a schematic of the experimental configuration that was used to measure the temperature profiles inside the porous media and the pollutant emissions concentrations. The burner consisted of four components: the porous media (h), a cavity for inserting an insulating ceramic mat (f), a slit for inserting the thermocouples (l) and a mixing chamber (e). The porous media consisted of a cylindrical ceramic honeycomb that was 64 mm in diameter with a nominal cell density of 400 square cells per square inch. The hydraulic diameter of the unit square cell was 0.75 mm, and the fraction of the open frontal area was 34.8%. The ceramic consisted primarily of alumina and had a thickness of 25 mm.

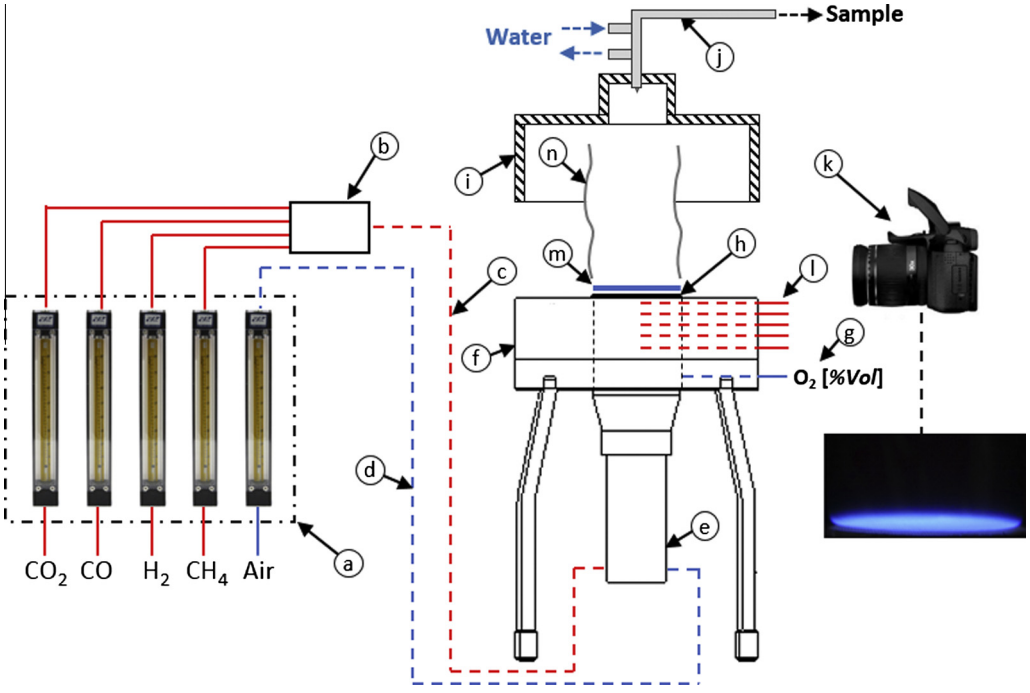

Fig. 2. Schematic of the experimental setup used to measure the temperature profiles inside the porous media and pollutant emissions concentration showing a – rotameters, b – fuel mixer, c – fuel line, d – air line, e – mixing chamber, f – cavity for inserting the insulating ceramic mat, g – mixture sample to verify aeration rate, h – porous media, i – chimney, j – probe, k – digital camera, l – slit for inserting thermocouples, m – flat flame and n – combustion products.

Table 1
Composition (%vol., dry) and properties of the fuel mixtures.

Components	SG	CH_4	CH_4–*SG*
H_2	55	–	27.5
CO	30	–	15
CO_2	15	–	7.5
CH_4	–	100	50
LHV	2.550	9.425	5.987
Wo	3.810	14.089	8.944
$V_{a,sto}$	2.023	9.520	5.712

The fuel and air entered the mixing chamber separately. High-purity certified gases (99% purity) were used to simulate the fuels: Table 1 lists the volumetric compositions and combustion properties of these gases. The combustion properties include the *LHV*, *Wo* and $V_{a,sto}$. The addition of *SG* to CH_4 in equimolar proportions reduced the *LHV* by 36.5% and $V_{a,sto}$ by 40%. The Wobbe Index (*Wo*) is used as the industry-standard gas interchangeability parameter because it indicates the relative amount of energy flowing through a section. Acceptable modifications to the *Wo* vary by country but generally fall between ±3% and ±10% [27]. In this study, the *Wo* value decreased by 36.52% when syngas was added to CH_4.

The air was supplied by an air compressor and dried using two inline water traps. Each air-to-fuel ratio and thermal input were ensured using rotameters that were specifically calibrated for each component gas, similar to those used in [28,29]. The errors in the final composition were estimated to be lower than 2%. Fig. 2 shows that the fuel component streams (H_2, CO, CO_2 and CH_4) were joined in the fuel line using an external mixer device (b).

A chimney (*i*) was placed at the top of the burner to facilitate the sampling by a water-cooled stainless-steel probe (*j*) to measure the O_2, CO, CO_2, and NOx concentrations in the combustion products. The sample was cleaned and dried before reaching the analyzers. The analytical instrumentation included a paramagnetic analyzer for the O_2 measurements, non-dispersive infrared gas analyzers (SICK MAIHAK s710 analyzers) for the CO and CO_2 measurements and a chemiluminescent analyzer for the NOx measurements (THERMO SCIENTIFIC 42i-HL analyzer). The relative measurement errors were 6% for CO, 3% for CO_2, 3% for O_2 and approximately 5% for NOx. Air dilution of the samples required that the CO emissions be adjusted to yield air-free measurements. This adjustment was performed by substituting the measured CO_2 emissions into the following equation.

$$CO_{air-free} = CO_{2max}(CO/CO_2)_{sample} \quad (2)$$

Due to the composition of the fuels used, it is expected that the addition of *SG* to CH_4 in equimolar proportion affects other important pollutants like unburned hydrocarbons and CO_2. However in this work only CO and NOx emissions are analyzed. These two pollutants are frequently cited as a significant cause of human diseases, especially at indoor conditions [30,31].

The temperature profiles within the porous media were measured using 33-μm wire-diameter S-thermocouples (T@0 mm and T@6 mm) and K-thermocouples (T@12 mm, T@8 mm and Tin) positioned along the centerline, as shown in Fig. 3. Thermal equilibrium was established among the thermocouple hot junction, the gas, and the solid phase; thus, the measurements provided by these sensors should be interpreted as the mean temperatures of the gas and solid phases. The desired air-to-fuel ratio and the thermal input were initially set with the flame ignited at the burner top. The flame front stabilized in the surface burner and heated the porous media, as indicated by the rising temperatures in the thermocouples for which the relative errors were approximately 1%.

The radiation efficiencies were investigated separately. Porous media without thermocouple perforations were used to measure the radiation efficiency to avoid radiation from the thermocouples. For this same reason, the chimney for collecting the combustion products was removed. The total radiative output was obtained by measuring the heat flux distribution using a similar method as that developed by Mital et al. [32,33]. In this method, the heat flux distribution is measured over a domain parallel to the burner surface, as shown in Fig. 4. A circular measurement domain was used because the burner had a circular shape, and the domain size was selected such that the heat flux measurements at the edge were close to the background values. To exploit symmetry, the circular plane was divided into four quadrants. The measurements were taken for only one quadrant, which was subdivided into smaller circles according to the size of the radiometer, as shown in Fig. 5 (i.e., heat flux measurements were taken in each of the smaller circles). The total radiant power output was obtained by multiplying the total heat flux by the area of the domain. The radiative flux was measured using a 14°-view-angle radiometer (Hukseflux Corporation, model SBG01). The transducer was a LI 19 (Hukseflux Corporation) with a relative error of approximately 4%. The radiometer was placed at a sufficient distance from the exhaust gases (L_R) to eliminate convective heat transfer. However, a water refrigeration system was used at the radiometer walls to isolate the radiometer from convective heat transfer; thus, the radiometer was only sensitive to the radiant energy input.

The radiation efficiency (n_R) is defined as the ratio between the total Po_{rad} and *Po*:

$$n_R = Po_{rad}/Po \quad (3)$$

To obtain various flame properties, such as the luminosity, structure and size, flame photographs and chemiluminescence photographs were directly captured using a digital camera and an ICCD camera, respectively. The ICCD camera was a 1024 × 1024-pixel *Princeton PI-MAX* and was equipped with a band-pass filter that was calibrated for the CH^* wavelength (387–430 nm). The exposure time was maintained constant to ensure that the digital and ICCD cameras had the same responsivity for all of the burner configurations.

3. Results and discussion

In this section, the experimental results are presented and discussed in four main subsections corresponding to the experimental configurations described in the previous section: the temperature profile, the radiation efficiency, the flame structure and CO and NOx emissions. The results in some subsections are used to explain the results from other subsections.

3.1. Temperature profile inside porous media

Fig. 6 shows the temperature profiles obtained in the porous media for $\lambda = 1.1$ and $\lambda = 1.4$ for operation at 1.0 kW, 1.8 kW and 2.5 kW using both CH_4 and CH_4–*SG*. For $\lambda = 1.4$ at 1.8 kW and 2.5 kW, stable flames could not be obtained for CH_4 and CH_4–*SG*. The distances shown in Fig. 6 were measured across the porous media, where 25 mm corresponds to the porous media inlet and 0 mm corresponds to the outlet surface.

The temperature increased significantly as the mixture passed through the porous media. The temperature measured at the burner outlet surface ranged between approximately 560 and 1000 K. However, at the porous media inlet, the temperature measurements varied by approximately 80 K between different tests because of radiation from the porous media.

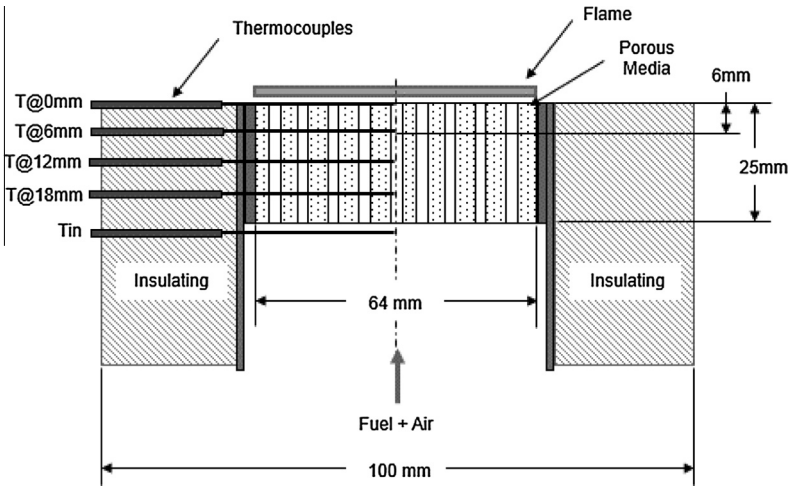

Fig. 3. Schematic of the temperature measurements.

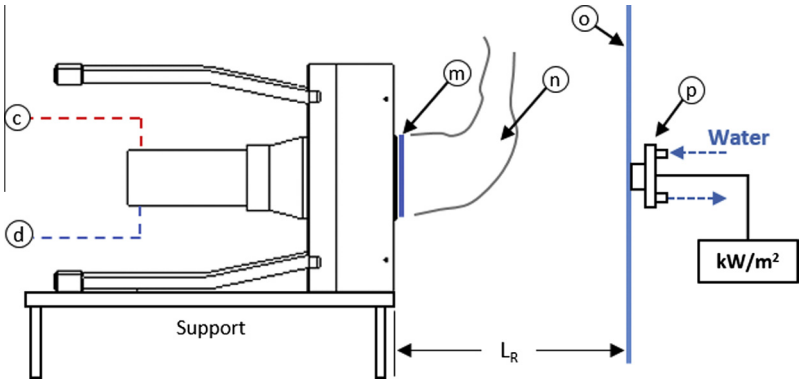

Fig. 4. Schematic of the experimental setup used to measure the radiation efficiency, c – fuel line, d – air line, m – flat flame, n – combustion products, o – measurement domain and p – radiometer.

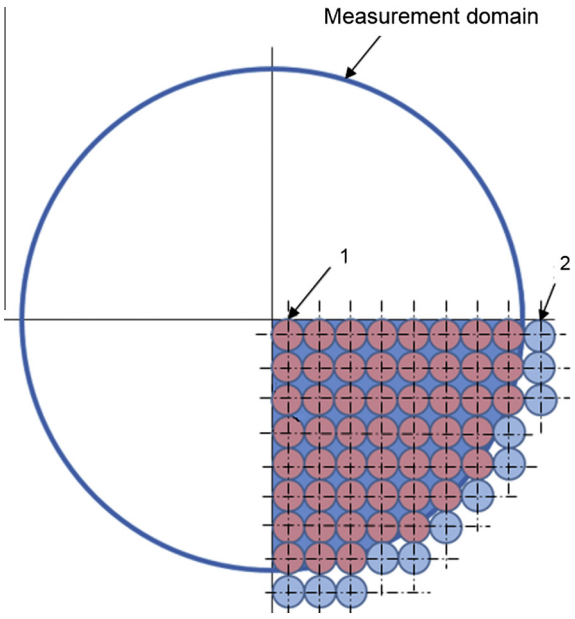

Fig. 5. Measurement domain of the radiative heat flux showing 1 – the measurement point and 2 – the measured value close to the background value.

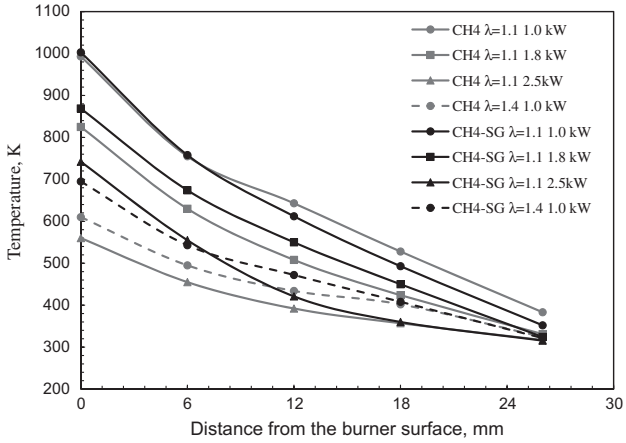

Fig. 6. Temperature profiles within the porous media for different fuels, aeration rates and thermal inputs. The distances are measured across the porous media, 25 mm corresponds to the porous media inlet and 0 mm corresponds to the outlet surface.

Adding *SG* to CH_4 reduced the *LHV* by 36.5% and $V_{a,sto}$ by 40%, as discussed in Section 2.2. Eq. (1) shows that using a CH_4–*SG* mixture with fixed λ and *Po* values should decrease V_U (see Table 2). Thus,

Table 2
The V_U and V_U/S_L for the fuels, the aeration rates and the thermal inputs.

Fuel	λ	*Po*	V_U	V_U/S_L
CH_4	1.1	1.0	30.44	0.89
CH_4–*SG*			30.43	0.69
CH_4	1.1	1.8	54.80	1.58
CH_4–*SG*			54.77	1.24
CH_4	1.1	2.5	76.11	2.20
CH_4–*SG*			76.06	1.72
CH_4	1.4	1.0	38.02	1.88
CH_4–*SG*			37.58	1.39
CH_4	1.4	1.8	68.44	3.38
CH_4–*SG*			67.65	2.51
CH_4	1.4	2.5	95.05	4.70
CH_4–*SG*			93.96	3.48

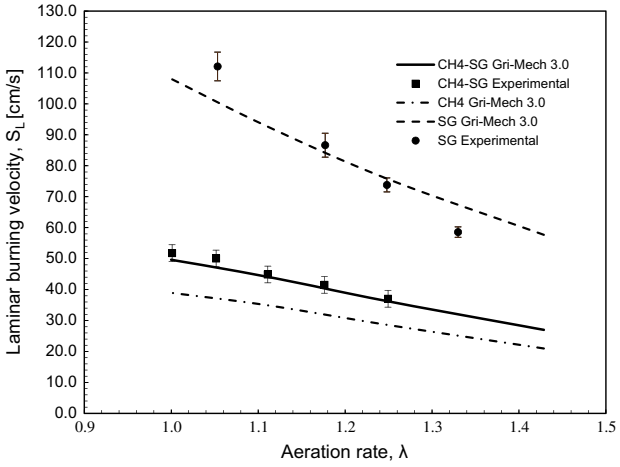

Fig. 7. Laminar burning velocities for CH_4, SG and CH_4–*SG*.

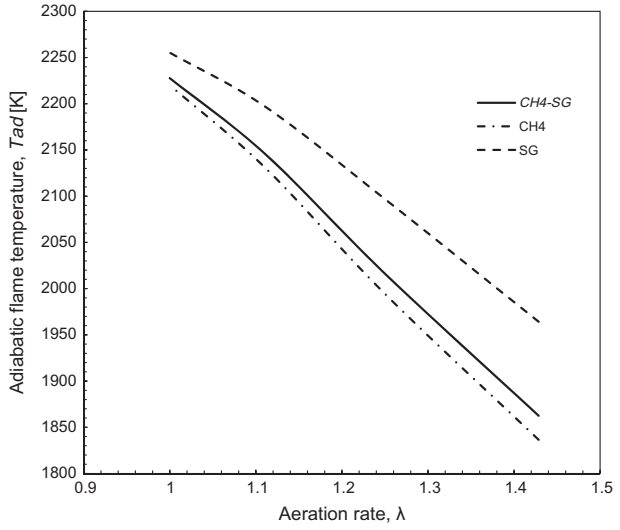

Fig. 8. Adiabatic flame temperatures for CH_4, SG and CH_4–*SG*.

and because of the high S_L and *Tad* of this high hydrogen *SG* compared to CH_4, variations in the temperature profile were expected. However, the differences were lower than expected, especially at λ = 1.1/1.0 kW, λ = 1.1/1.8 kW and λ = 1.4/1.0 kW. The similarities in the temperature profiles could be explained in terms of the laminar burning velocities and the adiabatic flame temperatures of the fuels.

Fig. 7 shows the numerical and experimental results for S_L for CH_4 and CH_4–*SG*. These results were obtained using the same numerical and experimental methodologies implemented in previous studies [28,34–36]. Fig. 8 shows the adiabatic flame temperature. The numerical calculations for S_L and *Tad* were performed using the *GriMech 3.0* reaction mechanism [37] and the *PREMIX* and *EQUIL* premixed flame codes from the *CHEMKIN-PRO* package at ambient temperature (298 K) and pressure (952 mbar). The experimental method was employed to confirm the reaction mechanism. Figs. 7 and 8 show S_L and *Tad* for *SG* to visualize the effect of both the fuels on the CH_4–*SG* mixture.

Figs. 7 and 8 show that adding *SG* to CH_4 produced a mixture that behaved similarly to CH_4 in terms of S_L and *Tad*. Recently, Park et al. [38] showed that the reactivity of a hydrocarbon–hydrogen mixture can be reduced because high amounts of methyl radicals produced from hydrocarbons can readily recombine with atomic hydrogen and reduce the rate of the $H + O_2 \rightarrow O + OH$ branching reaction, which in turn greatly affects the reactivity and hence, S_L and *Tad*.

The laminar burning velocity of CH_4–*SG* clearly increased over that of CH_4 but not as significantly as expected. Thus, the ratios V_U/S_L for CH_4 and CH_4–*SG* were slightly different and close to unity (see Table 2). The differences were approximately 10%, which did not appear to have a significant effect on the operation of the surface-stabilized burner in terms of the temperature profile at λ = 1.1/1.0 kW, λ = 1.1/1.8 kW and λ = 1.4/1.0 kW.

The difference in the temperature profile between CH_4 and CH_4–*SG* at λ = 1.1/2.5 kW can be explained by the high V_U/S_L ratio for CH_4, which indicates that V_U exceeded S_L by approximately two-fold, thereby reducing the heat losses from the flame to the burner surface compared to CH_4–*SG*. However, as we will discuss later, the visual appearances of the flames were similar.

At λ = 1.4/1.8 kW and λ = 1.4/2.5 kW, stable flames could not be obtained for CH_4 and CH_4–*SG*. At λ = 1.4/1.8 kW, the top view of the flames showed a cellular structure, and the side view showed a considerable detachment distance, as presented in the section on the flame structure (Section 3.3). At λ = 1.4/2.5 kW, the flames blew out. These two operation conditions for both fuels were attributed to the high V_U/S_L ratio, which were 2.5 and 4.7 for the lowest and highest cases, respectively.

As expected, increasing the thermal power decreased the preheating temperature for a given air-to-fuel ratio. This result can be explained by the increased V_U/S_L ratio that caused the flame front to move further downstream from the burner surface, as shown schematically in Fig. 1.

The increase in V_U for a given λ, A_{sup} and fuel composition meant that the thermal power could only be increased by increasing V_U, as shown by the following equation:

$$Po_{(2)} = Po_{(1)} \frac{V_{U,(2)}}{V_{U,(1)}} \tag{4}$$

The behavior of the temperature profile for λ = 1.4/1.0 kW and λ = 1.0/1.0 kW (which is shown using solid lines and circular markers, respectively, in Fig. 6) was as expected. The required thermal input for a given fuel composition and A_{sup} can be achieved using the following equation:

$$\dot{V}_{air(2)} = \lambda_{(2)} \frac{\dot{V}_{air(1)}}{\lambda_{(1)}} \tag{5}$$

For a constant thermal input and fuel composition, an increase in the air-to-fuel ratio implies an increase in the air flow rate ($\dot{V}_{air}$) and hence, an increase in V_U. S_L should also decrease, as shown in Fig. 8. Therefore, the V_U/S_L ratio increases and the burner surface temperature decreases, as explained in Section 2.1.

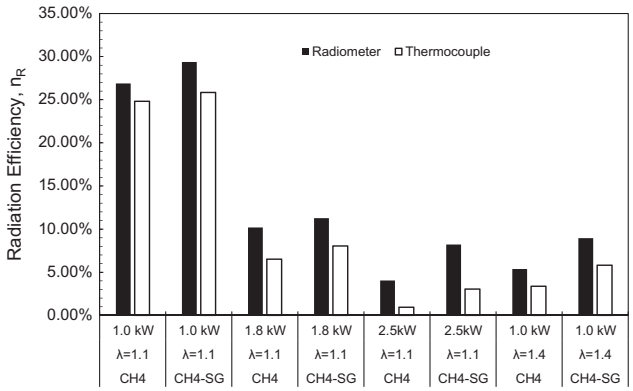

Fig. 9. The radiation efficiency of the fuels, the aeration rates and the thermal inputs.

3.2. Radiation efficiency

Fig. 9 shows the radiation efficiency that was obtained under the same operating conditions used to analyze the temperature profile. In addition to the radiometer methodology presented in Section 2.2, the radiation efficiency values calculated using Eq. (6) are presented to show the correlation between the temperatures reported in Section 3.1 and the radiation efficiencies obtained using the radiometer methodology.

$$n_R = \frac{A_{sup}\varepsilon\sigma(T_{sup}^4 - T_\infty^4)}{Po} \quad (6)$$

In Eq. (6), ε is the emissivity of the burner surface (which is assumed to be equal to the unit [12]), σ is the Stefan–Boltzmann constant, and T_{sup} was measured by the thermocouple placed at the center of the burner surface, as shown in Fig. 3 (T@0 mm).

The differences between the efficiencies determined using the radiometer methodology and Eq. (6) can be attributed to the surface temperature measured with the thermocouple, which does not correspond to the actual temperature of the solid phase, as explained in Section 2.2, and to neglecting the radiation from the flame. Additionally, the differences between methodologies increase as the thermal input increases. This behavior can be explained by the increase of the radiation from the flame, which is not registered by the thermocouple methodology and it is expected to increase because the flame temperature increases as explained in Section 2.1.

Adding *SG* to CH_4 decreased the V_U/S_L ratio, thereby increasing the surface temperature, as shown in Section 3.1, and the radiation. The radiation efficiency increased on the order of 1.08–3.58 efficiency points, corresponding in some cases (λ = 1.1/2.5 and 1.4/1.0 kW) to an increase of ~66% relative to the results obtained for CH_4.

However, the increase in the thermal power and the air-to-fuel ratio considerably reduced the radiation efficiency, which can be explained by the decrease in the surface temperature of the porous media, as previously discussed.

3.3. Flame structure

Parameters such as the color, structure and stability of the flame, which depend on λ and *Po*, were observed and recorded with a digital camera, as shown in Fig. 10 for CH_4.

Fig. 10a shows that at λ = 1.1/1.0 kW, an outer yellow mantle extended downstream from the flame front. This mantle was not observed under the other conditions, as shown in Fig. 10b–e and 10a; thus, it was possible to observe a primary reaction zone close to the burner surface. This phenomenon could be explained by the generation of a secondary reaction zone because of "*flame cooling*" from heat loss at the burner surface. This result was consistent with the other results obtained for this operating condition, including (a) the highest surface temperature reported in Fig. 6, (b) the highest radiation efficiency reported in Fig. 9, (c) the lowest V_U/S_L ratio reported in Table 2 and (d) the increase in CO emissions and the decrease in NOx emissions.

The small reaction zone was a very important feature of the surface-stabilized combustion in the porous media (Fig. 10) and the displacement of the reaction zone for increasing λ and *Po*, especially at λ = 1.1/2.5 kW and λ = 1.4/1.8 kW, as shown in Fig. 10c and e, respectively.

Adding *SG* to CH_4 did not change the appearance of the flame. The color, stability and structure of the flame were not significantly altered when *SG* was added to CH_4. This result was probably obtained because S_L and *Tad* had similar values for both CH_4 and CH_4–*SG*. However, a slight change in luminosity was observed that could not be properly identified by the conventional photographic register. Thus, a chemiluminescence photographic record of the CH^* radical was used.

The luminosity of a flame is attributed to the emission of light from excited radicals in the reaction zone. The chemiluminescence method can be used to identify the flame front with great precision and to determine the heat release rate of a flame because any decrease in the temperature or "*reactivity*" of the reaction zone involves a reduction in the emission of chemical species [39,40].

Fig. 11 is a top view from the photographic records of the intensity distribution over the wavelength range of the CH^* radical. The colors have been ordered from the highest to the lowest intensities as follows: red, yellow, green, blue-green, blue and black.

Note that to qualitatively analyze these images, the exposure times and the maximum intensity values of the ICCD camera had to be maintained constant because the camera assigned a maximum value to the point at which the highest emission wavelength was recorded, and the image collection was based on this maximum value to assign values to the other emission sources. That

Fig. 10. Direct flame photographs for CH_4: (a) λ = 1.1/1.0 kW, (b) λ = 1.1/1.8 kW, (c) λ = 1.1/2.5 kW, (d) λ = 1.4/1.0 kW, (e) λ = 1.4/1.8 kW and (f) λ = 1.4/2.5 kW.

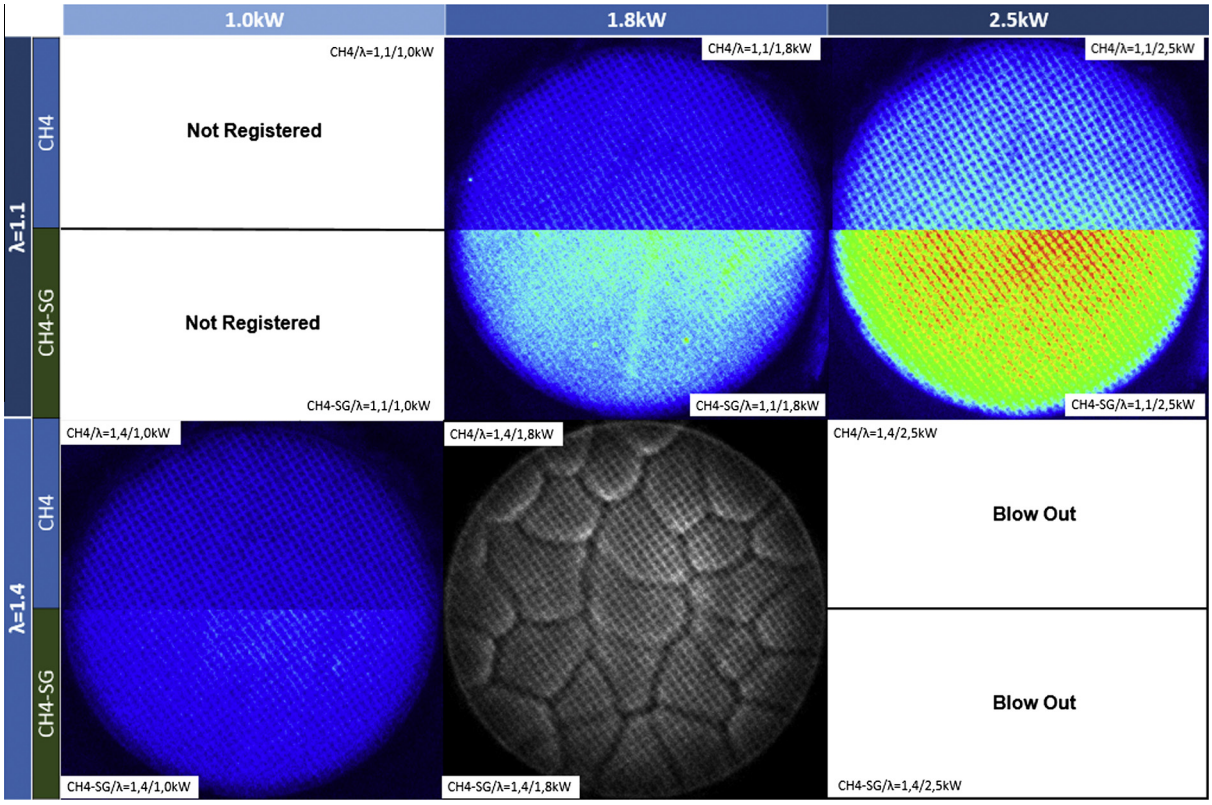

Fig. 11. Top view of the photographic record of the intensity distribution in the wavelength range of the radical CH^* for different fuels, aeration rates and thermal inputs.

is, the same intensity scale was used in this process so that different images could be compared to each other.

Fig. 11 shows that the intensity increased with the thermal power input. This result can be explained by the fact that increasing the power of the thermal input decreased the heat transferred to the burner surface (see Figs. 6 and 9). Therefore, the temperature at the flame front increased, and the total CH^* emission intensity increased.

The increase in the fuel flow rate also explains the increase in the intensity of the images for CH_4–*SG* relative to that in the images for CH_4. Adding *SG* to CH_4 increased the reactivity of the mixture, as shown by the increase in S_L in Fig. 8.

Fig. 11 illustrates the instabilities obtained for $\lambda = 1.4/1.8$ kW for both fuels. The image is presented in gray scale so that the instabilities can be more clearly visualized. Fig. 10e shows that these instabilities were characterized by a cellular structure, as shown in the top view, and by a considerable detachment distance, as shown in the side view.

3.4. CO and NOx emissions

Figs. 12 and 13 show the pollutant emissions (CO and NOx) for the fuels for different air-to-fuel ratios (λ) and thermal load inputs for the surface-stabilized combustion burner. Adding *SG* to CH_4 increased the CO emissions and decreased the NOx emissions compared to those for CH_4. At $\lambda = 1.1/2.5$ kW and $\lambda = 1.4/1.0$ kW, the increase in the CO emissions and the decrease in the NOx emissions was on the order of 100% and 50%, respectively. However, the emission concentrations were very low in both cases. This behavior can be explained in terms of the heat loss from the flame to the porous media, which was higher for CH_4–*SG*, as evidenced by the increase in the porous media temperature profile in Fig. 6 and the increase in the radiation efficiency in Fig. 9. Therefore, the CH_4 flame temperatures were expected to be higher than the CH_4–*SG* flame temperatures. In many practical applications, the oxidation of CO to CO_2 has been shown to occur in the latter stages of combustion via several chemical routes that are strongly temperature-dependent. For example, for a chemical route that is known as the "wet route" because of the presence of the OH radical, as shown in Eq. (7), the oxidation of CO depends strongly on the OH radical concentration that is produced principally by the branching reaction $H + O_2 \rightarrow OH + O$, which practically stops for temperatures below 1100 K.

$$CO + OH \rightarrow CO_2 + H \tag{7}$$

However, the formation of NOx, particularly NO, has been shown to be strongly temperature-dependent and tends to increase under slightly poor conditions where the flame temperature is high and O_2 is available [41].

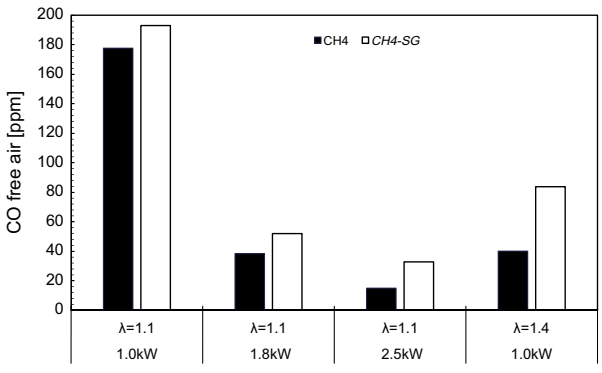

Fig. 12. CO emissions of the stable flames.

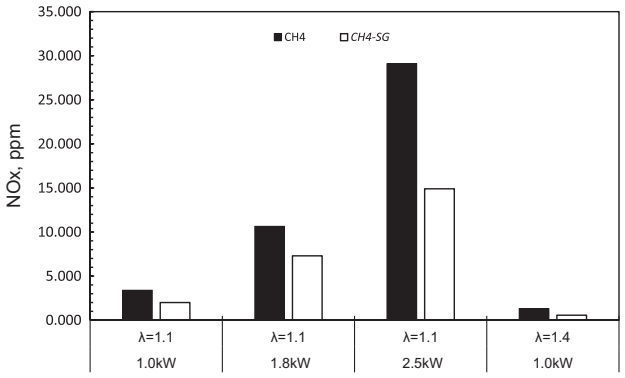

Fig. 13. NOx emissions of the stable flames.

At $\lambda = 1.1/1.0$ kW and $\lambda = 1.1/1.8$ kW, the differences between the CH_4 and CH_4–*SG* results were small because the flame temperatures were very similar at these conditions, as evidenced by the similarities observed for *Tad* (see Fig. 8), the temperature profiles inside the porous media (see Fig. 6) and the radiation efficiencies (see Fig. 9). These slight differences could be attributed to the reduction in the quantity of air when *SG* was added to CH_4.

The pollutant emissions were highly susceptible to variations in the thermal inputs and the air-to-fuel ratios. Similarly, as previously explained, decreases of up to 91% for CO emissions and increases of up to 83.93% for the NOx emissions resulted from the increase in the flame temperature. These results can be inferred from Figs. 6 and 9, which show that the burner temperature profile and radiation efficiency decreased with increasing *Po* and λ. Therefore, the reduction in the heat loss from the flame to the burner surface was to be expected.

However, the high CO emission for $\lambda = 1.1$ at 1.0 kW can be explained in terms of the aforementioned flame cooling hypothesis, which resulted from the low V_U/S_L ratio that caused the flame to come into close contact with the burner surface, thereby increasing the heat loss.

4. Conclusions

The performance of a ceramic porous media burner operating in a surface combustion mode was studied for two different fuels, CH_4 and an equimolar mixture of CH_4 and a high-content H_2/CO syngas. The following conclusions can be drawn from the results of adding *SG* to CH_4 in equimolar proportions.

- From a macro perspective that includes the temperature profile inside the porous media, the radiation efficiency and the flame structure, the surface-stabilized combustion burner exhibits considerable potential for the interchangeable use of gas fuels. Compared to CH_4-only operation, the addition of *SG* affected the temperature profile inside the porous media, the radiation efficiency and the flame structure. Differences in the temperature profile and the radiation efficiency were observed for $\lambda = 1.1/2.5$ kW and $\lambda = 1.4/1.0$ kW. However, these differences were not noticeable by visual inspection.
- CO emissions were found to increase by ~9–107% and NOx to decrease by 31–56%.

The following conclusions can be drawn from the variations in the thermal input and the air-to-fuel ratio.

- The air-to-fuel ratio had a considerable effect on the radiation efficiency, the pollutant emissions, the flame structure and the temperature profile within the porous media. An increase of 0.3 points in the air-to-fuel ratio decreased the temperature inside the porous media, thereby reducing the radiation efficiency to ~80%. This result can be explained by the increase in the V_U/S_L ratio.
- Pollutant emissions were highly influenced by the thermal power input. For the geometrical configuration used in this study, increasing the thermal input decreased the CO emissions up to ~91% and increased the NOx emission up to ~84%. This result can be explained by the increase in the flame temperature because of the reduction in the heat losses from the flame to the burner surface.
- For optimal operation with low pollutant emissions and high flame stability, the burner control system can be used to simultaneously vary the air-to-fuel ratio and the thermal input.

Acknowledgements

The authors would like to acknowledge the "*Programa de sostenibilidad de laVicerrectoria de Investigación de la Universidad de Antioquia 2013 - 2014*" and *COLCIENCIAS* for their valuable economic contributions to the project "Estudio de la combustión en medios porosos del gas natural, g.l.p, biogas y syngas a diferentes altitudes".

References

[1] Colorado AF, Herrera BA, Amell AA. Performance of a flameless combustion furnace using biogas and natural gas. Bioresour Technol 2010;101:2443–9.
[2] Jones HRN. The application of combustion principles to domestic gas burner design. Taylor & Francis; 1989.
[3] Ko Y-C, Lin T-H. Emissions and efficiency of a domestic gas stove burning natural gases with various compositions. Energy Convers Manage 2003;44:3001–14.
[4] NATURGAS. La Meta de un millón de nuevos hogares usuarios de gas está cerca. Marzo; 2013.
[5] UPME. Proyección de Demanda de Energía Eléctrica en Colombia; 2013.
[6] Casleton KH, Breault RW, Richards GA. System issues and tradeoffs associated with syngas production and combustion. Combust Sci Technol 2008;180:1013–52.
[7] Richards G, McMillian M, Gemmen R, Rogers W, Cully S. Issues for low-emission, fuel-flexible power systems. Prog Energy Combust Sci 2001;27:141–69.
[8] Chaos M, Dryer FL. Syngas combustion kinetics and applications. Combust Sci Technol 2008;180:1053–96.
[9] Vélez JF, Chejne F, Valdés CF, Emery EJ, Londoño CA. Co-gasification of Colombian coal and biomass in fluidized bed: an experimental study. Fuel 2009;88:424–30.
[10] Giles DE, Som S, Aggarwal SK. NOx emission characteristics of counterflow syngas diffusion flames with airstream dilution. Fuel 2006;85:1729–42.
[11] Wood S, Harris AT. Porous burners for lean-burn applications. Prog Energy Combust Sci 2008;34:667–84.
[12] Francisco RW, Rua F, Costa M, Catapan RC, Oliveira AAM. On the combustion of hydrogen-rich gaseous fuels with low calorific value in a porous burner. Energy Fuels 2010;24:880–7.
[13] Mujeebu MA, Abdullah MZ, Bakar MZA, Mohamad AA, Muhad RMN, Abdullah MK. Combustion in porous media and its applications – a comprehensive survey. J Environ Manage 2009;90:2287–312.
[14] Marbach TL, Agrawal AK. Experimental study of surface and interior combustion using composite porous inert media. J Eng Gas Turbine Power 2005;127.
[15] Dunn-Rankin D, Cheng RK, Levinsky H. Lean premixed burners. Lean Combust 2008;0. 161–V.
[16] Lammers F. Ceramic-foam surface burners in high-temperature environments. Int J Prod Econ – INT J PROD ECON; 2001.
[17] Goverse H. Single digit NOx emissions with ceramic foam burners. Int Conf Atmos Pollut NOx N20 Emiss. Control panel available Tech., Paris (France); 2001.
[18] Marbach TL, Sadasivuni V, Agrawal AK. Investigation of a miniature combustor using porous media surface stabilized flame. Combust Sci Technol 2007;179:1901–22.
[19] Mujeebu MA, Abdullah MZ, Mohamad AA. Development of energy efficient porous medium burners on surface and submerged combustion modes. Energy 2011;36:5132–9.
[20] Yu B, Kum S-M, Lee C-E, Lee S. An experimental study of heat transfer and pollutant emission characteristics at varying distances between the burner and the heat exchanger in a compact combustion system. Energy 2012;42:350–7.

[21] Yu B, Kum S, Lee C, Lee S. Combustion characteristics and thermal efficiency for premixed porous-media types of burners. Energy 2013;53:343–50.
[22] Keramiotis C, Stelzner B, Trimis D, Founti M. Porous burners for low emission combustion: an experimental investigation. Energy 2012;45:213–9.
[23] Wu C-Y, Chen K-H, Yang SY. Experimental study of porous metal burners for domestic stove applications. Energy Convers Manage 2014;77:380–8.
[24] Dyk JC Van, Keyser MJ, Coertzen M. Syngas production from South African coal sources using Sasol – Lurgi gasifiers 2006; 65: 243–53.
[25] Hermann H, Reinhard R, Reinhard K, Crhistian A. Biomass CHP Plant Güssing – a success story. Vienna; 2001.
[26] Bouma P. Methane –air combustion on ceramic foam surface burners. Technische Universiteít Eindhoven; 1997.
[27] International Gas Union, Petroleum B. Guidebook to gas interchangeability and gas quality; 2011.
[28] Burbano HJ, Pareja J, Amell AA. Laminar burning velocities and flame stability analysis of syngas mixtures at sub-atmospheric pressures. Int J Hydrogen Energy 2011;36:3243–52.
[29] Burbano HJ, Pareja J, Amell AA. Laminar burning velocities and flame stability analysis of H_2/CO/air mixtures with dilution of N_2 and CO_2. Int J Hydrogen Energy 2011;36:3232–42.
[30] Junus R, Stubington JF, Sergeant GD. The effects of design factors on emissions from natural gas cooktop burners. Int J Environ Stud 1994;45:101–21.
[31] Jarvis D, Chinn S, Luczynska C, Burney P. Association of respiratory symptoms and lung function in young adults with use of domestic gas appliances. Lancet 1996;347:426–31.
[32] Mital R, Gore JP, Viskanta R. A radiation efficiency measurement procedure for gas-fired radiant burners. Exp Heat Transf 1998;11:3–21.
[33] Mital R, Gore JP, Viskanta R, Mcintosh AC. An experimental evaluation of asymptotic analysis of radiant burners. Symp Combust 1998;27:3163–71.
[34] Cardona CA, Amell AA. Laminar burning velocity and interchangeability analysis of biogas/C3H8/H2 with normal and oxygen-enriched air. Int J Hydrogen Energy 2013;38:7994–8001.
[35] Yepes HA, Amell AA. Laminar burning velocity with oxygen-enriched air of syngas produced from biomass gasification. Int J Hydrogen Energy 2013;38:7519–27.
[36] Pareja J, Burbano HJ, Amell A, Carvajal J. Laminar burning velocities and flame stability analysis of hydrogen/air premixed flames at low pressure. Int J Hydrogen Energy 2011;36:6317–24.
[37] Smith G, Glden D, Frenhlach M, Moriaty NW. GRI-Mech 2000;3.
[38] Park O, Veloo PS, Liu N, Egolfopoulos FN. Combustion characteristics of alternative gaseous fuels. Proc Combust Inst 2011;33:887–94.
[39] Kathrotia T, Riedel U, Warnatz J. A numerical study on the relation of OH^*, CH^*, and $C2^*$ chemiluminescence and heat release in premixed methane flames. In: 4th Proc Eur Combust Meet, Vienna University of Technology, Vienna, Austria; 2009.
[40] Hossain A, Nakamura Y. A numerical study on the ability to predict the heat release rate using CH^* chemiluminescence in non-sooting counterflow diffusion flames. Combust Flame 2013.
[41] McAllister S, Chen J-Y, Fernandez-Pello AC. Fundamentals of combustion processes. Springer; 2011.